

CHAPTER 7

EMPIRICAL MODE DECOMPOSITION AND CLIMATE VARIABILITY

Katie Coughlin and Ka Kit Tung

Empirical mode decomposition (EMD) is used to extract inter-annual atmospheric signals. Our climate contains components that are often distinguished from one another on temporal, rather than spatial, scales, and EMD is found to be a useful tool in extracting physically meaningful information from the data. The National Centers for Environmental Prediction has provided reanalyzed data, which are used here to demonstrate that dynamical variables in the zonally averaged troposphere and lower stratosphere contain only five oscillating modes and a trend. These oscillations contain interesting amplitude and frequency modulations which are cumbersome and difficult to interpret when viewed in the traditional Fourier frequency domain. EMD analysis provides a unique, relatively unbiased and useful way to decompose the time series. Statistical tests are developed to determine the confidence in our analysis. Physical interpretations of the significant modes are also discussed with corresponding justification. By combining the information found for the time series of each horizontal strip into a spatial matrix, valuable spatial information about these physical processes have been obtained.

7.1. Introduction

Empirical mode decomposition (EMD) can be a useful time series analysis tool, particularly for analyzing the climate records of the atmosphere beyond annual time scales. Global climate phenomena are often separated in temporal, rather than spatial, scales. Therefore, time series analysis is more appropriate for the initial decomposition of climate data than spatial methods, which have previously been used to find climate components. Furthermore, nonlinear trends, irregular frequencies and amplitude modulations, which are inherently present in these physical phenomena, make EMD especially appropriate for this problem.

Understanding the variability of our climate is important. Atmospheric variability on inter-annual time scales is investigated here with a focus on observations in the regions which most influences us; the lower stratosphere ($\sim 12 - 30$ km) and the troposphere (0–12 km). The main difficulty is disentangling the atmospheric signals in these regions. In both the stratosphere and the troposphere, inter-annual signals are mixed with one another as well as with noise. Isolating the relevant signals is a daunting task. Traditional time-series techniques, based on Fourier transforms, tend

to spread the signal energy into multiple frequency bins which sometimes leads to ambiguous interpretations of the data. Other methods, such as empirical orthogonal function (EOF) analysis, depend on spatial decompositions to filter the noisy data. However, as mentioned above, the signals of interest are mostly global in extent and distinguishable from one another temporally, not by their spatial scales. EOF analysis leads to a leading mode which contains climate signals of various time scales projected — unphysically — onto a spatial pattern which contains the most variance. Long period climate oscillations, which usually have a smaller variance than other oscillations, are either grossly distorted or missing altogether in the leading EOFs. There is no real reason why a spatial decomposition should isolate temporal signals. Here, we use the empirical mode decomposition (EMD) method, Huang et al. (1998) designed for time series analysis. The modes generated by this method are derived directly from the data. Here, we show that the atmospheric signals in the stratosphere and troposphere can be completely decomposed into five of these oscillating modes: an annual cycle, a Quasi-Biennial Oscillation (QBO) signal, an El Niño/Southern Oscillation (ENSO)-like mode and a solar cycle mode. The last mode is a trend which indicates cooling in the stratosphere and warming in the troposphere, as expected from the recent increase in greenhouse gases. Statistical tests, used to determine the significance of these EMD modes, will also be discussed here.

7.2. Data

Atmospheric measurements are often made from balloons and aircraft with reference to pressure levels instead of height, since the pressure can be measured more accurately in situ. The analysis shown here is plotted on pressure surfaces, measured in hecto-Pascals (hPa).** The pressure decreases as the distance from the surface increases and provides a useful axis for looking at atmospheric dynamics.

The monthly averages of the NCEP Daily Global Analyses data are provided by the NOAA-CIRES Climate Diagnostics Center in Boulder, Colorado, USA, available on line at <http://www.cdc.noaa.gov/> (Kalnay et al. 1996). These averages are used here to create a time series of geopotential height from January 1958 to July 2002. A spatial average of the total geopotential height from 20°N to 90°N is performed at 17 levels, from 10 hPa down to 1000 hPa. This averaged Northern Hemisphere time series is decomposed by using the EMD method, and the results are analyzed here. To investigate the latitudinal dependence, zonally averaged latitudinal strips of the total geopotential height are decomposed and analyzed as well. A typical tropospheric (stratospheric) decomposition of the total geopotential height at 700 hPa (30 hPa), averaged from 20°N to 90°N, is shown in Fig. 7.1. The results for all 17 levels show similar decompositions of the five modes, each with a variable amplitude and period, and a trend.

** A hPa is equivalent to a mbar where pressure at the surface of the earth is $\sim 1 \text{ bar} = 1000 \text{ mb} = 1000 \text{ hPa}$.

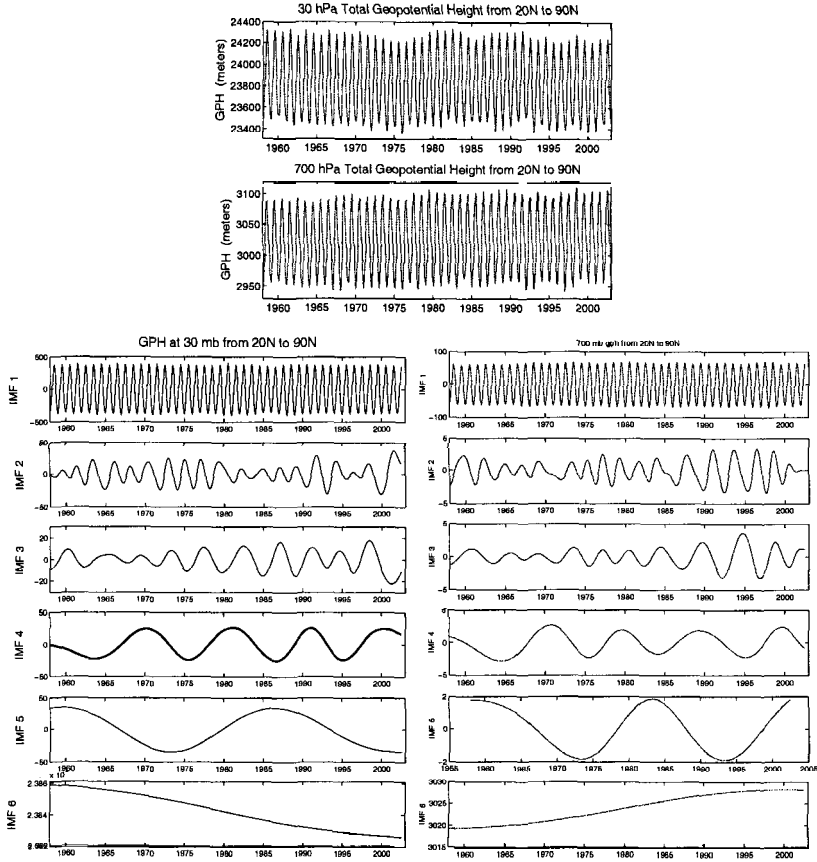


Figure 7.1: *Top.* The total geopotential height at 30 hPa and 700 hPa spatially averaged over 20°N to 90°N . *Bottom.* The decomposition of the 30 hPa (left) and 700 hPa (right) geopotential height produces five modes and a trend. The first mode is the annual cycle. The second mode is the extratropical QBO, with an average period of 28 months. The third ENSO-like mode has an average period of around four years, and the fourth mode is highly correlated with the 11-yr sunspot cycle. We refrain from commenting on the 22-yr mode found since the data record contains only two periods of this oscillation. The trend in recent decades indicates cooling in the troposphere and warming in the stratosphere. This finding is consistent with the anticipated effect of the increase in greenhouse gases. Figure 7.1 was taken from Coughlin, K. T., and K. K. Tung, 2004: 11-year solar cycle in the stratosphere extracted by the empirical mode decomposition method. *Adv. Space Res.*, **34**, 323–329 with permission.

The sunspot record is provided by the SIDC, RWC Belgium, World Data Center for the Sunspot Index, Royal Observatory of Belgium, available on line at <http://sidc.oma.be/>. This record consists of monthly data from January 1749 to September 2002. Only the data from 1958 to 2002 are utilized here.

The data used to characterize the QBO winds are from personal email communications with Barbara Naujokat. As one of the compilers of the daily stratospheric charts at the Stratospheric Research Group of the Free University Berlin, she tab-

ulated the daily wind observations of selected stations near the equator since 1957. For the earlier years, the values were extracted from the Northern Hemisphere Data Tabulations. From these daily values, the monthly mean zonal wind components were calculated for the levels 70, 50, 40, 30, 20, 15, and 10 hPa, and a dataset from 1953 to the present was produced by combining the observations from the three radiosonde stations; Canton Island (closed 1967), Gan/Malediva Islands (closed 1975), and Singapore. The negative values are easterly (from the east), and the positive values are westerly. This dataset is supposed to represent the equatorial belt since all studies have shown that the longitudinal differences in the phase of the QBO are small. However, some uncertainties arose at higher levels during the early years because of the scarcity of observations. More information on the data can be found in Naujokat (1986).

The Multivariate ENSO Index (MEI) bimonthly time series from Dec/Jan 1949/1950 up to Nov/Dec 2003 is used as a robust measure of the ENSO. More information on the MEI can be found on the MEI homepage, available online at www.cdc.noaa.gov/~kew/MEI/mei.html, and in Wolter (1987) and Wolter and Timlin (1993,1998).

7.3. Methodology

Climate signals in the atmosphere are often lost among the noise and data-collection and assimilation problems. Although climate signals are recognized mainly by their time scales, previous analysis, such as the use of empirical orthogonal functions (EOFs), relies on spatial decompositions to remove excess noise. In some cases, this method is useful, but in general, there is no *a priori* reason to expect temporal signals to be defined in terms of spatial patterns ordered by their variances (as required by EOF analysis). In fact, time series analysis is more appropriate for the decomposition of climate signals. The traditional time series analysis tools usually rely on Fourier transforms in one way or another. However, Fourier transforms lead to inconclusive interpretations due mainly to the global nature (in the time domain) of the transforms. Even wavelet analysis, developed to deal with non-stationarity and local frequency changes, produces confusing and sometimes contradictory results when applied to climate signals (Mak 1995; Oh et al. 2003; Sonechkin and Datsenko 2000). These three papers all use similar types of wavelet analysis on global, surface climate data and obtain three different results. With wavelet analysis, it is sometimes difficult to distinctly define local frequency changes because the spectra are created by stepping through various predetermined frequencies, often producing a blurred result. Wavelets have the additional problem of shift variance. If the starting point is varied by dropping the initial point, for example, wavelet analysis can produce completely different results. In comparison, the EMD method makes no assumption about linearity or stationarity, and the intrinsic mode functions (IMFs) are usually easy to interpret and relevant to the physical system being studied (see Flandrin et al. 2004; Huang et al. 1998, 1999; Zhu et al. 1997 for further discussion of the method and comparison to other time series analysis techniques).

EMD must be used cautiously even though it is a powerful method. One difficulty encountered when using it is the sensitivity to end point treatments. The envelopes are calculated by using a cubic spline; however, splines are notoriously sensitive to end points. The end effects must not be allowed to propagate into the interior solution. As described in Coughlin and Tung (2004a), this problem is dealt with by extending both the beginning and end of the data by the addition of typical waves,

$$\text{wave extension} = A \sin(2\pi t/P) + \text{phase} + \text{local mean} . \quad (7.1)$$

The typical amplitude A and period P are determined by the nearest local extrema; i.e.,

$$A_{\text{beginning}} = \frac{1}{2} \|\max(1) - \min(1)\| , \quad (7.2)$$

$$A_{\text{end}} = \frac{1}{2} \|\max(N) - \min(N)\| , \quad (7.3)$$

$$P_{\text{beginning}} = 2 \|\text{time}(\max(1)) - \text{time}(\min(1))\| , \quad (7.4)$$

$$P_{\text{end}} = 2 \|\text{time}(\max(N)) - \text{time}(\min(N))\| , \quad (7.5)$$

where $\max(1)$ and $\min(1)$ are the first two local extrema in the time series, and $\max(N)$ and $\min(N)$ are the last two local extrema. This calculation takes place every iteration so that the additional waves are continually changing in amplitude and frequency. Because the additional waves have the same amplitude as the nearest oscillations, the addition of these waves causes the slope of the envelope to tend toward zero at the beginning and end of the time series. This technique eliminates large swings in the spline calculation that may otherwise form when the slope is artificially forced to zero. Two or three oscillations of approximately the same amplitude are needed in order to flatten the spline. Any more than this can adversely affect the low frequency modes by artificially leveling the ends of any long-term trend present in the data.

The stopping criterion is another issue that can affect the decomposition. In order to allow more natural flexibility in the modes, we stop the sifting process and define a mode when the number of extrema is equal to or one different from the number of zero crossings (our criterion is similar to the one suggested in Huang et al. 1999). We also require this condition to be consistent for three iterations in a row in order to constrain the local means to be close to zero. If the Hilbert transform is to be used on the subsequent modes, a stricter condition on the local mean may be useful since the Hilbert transform is very sensitive to changes in this mean. In our analysis, however, we compare the modes directly to physically relevant oscillations and are less concerned with a precise zero mean.

Another important component of the analysis, as described in Coughlin and Tung (2004a), is the inclusion of the annual cycle. Unlike more traditional methods, where a twelve-month climatology is subtracted from the data and only the

anomalies are studied, this method decomposes the total atmospheric signal, not just the anomalies. In fact, the removal of climatology, which is a linear operation, can actually degrade the nonlinear analysis. Here, the annual cycle is an important component and is retrieved as the first IMF in the decomposition. In some cases, a three-month running average can be applied to the time series to damp month-to-month variations and retrieve the annual cycle as our first mode. These higher month-to-month frequencies are either intermittent or appear to be intermittent. In either case, the resulting modes contain a mixture of frequencies, and these mixed modes are much more difficult to interpret than other modes. Since we are not interested in intraseasonal variations, a minimal amount of pre-smoothing is performed so that the first mode will contain the annual cycle. Since the annual cycle is relatively small near the equator, where the seasons are less distinct, we expected our results to be somewhat degraded in this region due to the pre-smoothing process that takes place there, but surprisingly, we find that the equatorial signals remain relatively robust in most cases.

The IMFs will generally be ordered from high to low frequency, and the last IMF often contains a trend. The significance of the IMFs must be determined. We should not expect all modes to be significant.

7.4. Statistical tests of confidence

The significance of the EMD modes must be calculated. Our confidence in these modes can be tested by comparing their energy spectra to the energy spectrum of decomposed noise. Our statistics are developed specifically for this climate problem (see Coughlin and Tung 2004a).

To distinguish the signals from noise in the EMD method is used, we examine the energy of all the IMFs and compare the energy in each mode to the energy distribution of red noise. Typically, we may expect the highest frequency mode to contain only noise, so the power in this mode can then be used to calibrate the noise distribution. However, in this case, the first mode contains a climatological annual cycle, which obviously does not contain pure noise. To estimate the power of the noise present in this time series, we subtract the climatology from the first mode and assume that the remainder is noise. This estimate of the noise is still very conservative. However, by using this criteria, we can normalize the red noise spectrum and perform a Monte-Carlo simulation to test the significance of the remaining IMFs. In atmospheric phenomena, the data at one time step tend to be related to the data at the previous time step. For example, the temperature on a day (or month) will be similar to the temperature on the day (or month) before. This similarity is called "persistence," and this "redness" or autocorrelation should be accounted for when creating Monte-Carlo simulations to test the significance of the decomposition. In our simulations Coughlin and Tung (2004a,b), we create 500 random "red" time series with the same autocorrelation as that of the difference between the data and the climatology. The variance of these time series is calculated

based on the “noise” in the first mode, which is found by subtracting the climatology from the first mode, and then the original climatology is added back into each of these time series before using EMD to define their modes. In this way, the first mode contains the annual cycle, and the power of the original remaining modes can then be compared to the power in the modes created from the red noise. The red noise, or random time series, is

$$\text{rts}(t_n) = A_{\text{noise}}E(t_n) + \rho \text{rts}(t_{n-1}), \quad (7.6)$$

$$A_{\text{noise}} = \text{standard deviation (IMF1 - climatology)}, \quad (7.7)$$

and

$$\rho = \text{autocorrelation of (total geopotential height - climatology)}, \quad (7.8)$$

where E contains a uniform distribution of random numbers with values between 1 and -1 , t_n is the n th time step, and rts is the random time series generated. The climatology is the geopotential height averaged over all years of the data record for each individual month and is added to the random time series before applying the EMD method.

EMD modes are generated by using these time series, and then the statistics of this simulation are calculated to create the energy distribution of the noise. The power of each IMF is then compared to this distribution to determine its significance.

In Fig. 7.2, the average power per period of modes 2, 3 and 4 in the 30-hPa and 700-hPa geopotential height is compared to that of modes 2, 3 and 4 of 500 randomly generated time series. These series are created by adding the 30-hPa, or 700-hPa, climatology to appropriately scaled red noise. For randomly generated time series, the EMD method exhibits a period doubling phenomenon so that each mode tends to have an average period of about twice that of the previous mode (as described in Flandrin et al. 2004). This result creates a clustering of the modes about certain periods in the Monte-Carlo plot (Fig. 7.2). The average power of the random modes varies inversely to that of the average period (power $\sim 1/\text{period}$) so that the modes quickly decrease in power as the average period increases. Here, the power per period is plotted, allowing one to directly compare each mode, so the points actually decrease in inverse proportion to the square of the period. The thick line is the linear least squares fit of the noise, and the dashed line is one standard deviation above this best fit line. The three stars represent the average power per period of IMF 2, IMF 3 and IMF 4 of the 30-hPa, or 700 hPa, geopotential height at average periods of 28, 59 and 132 months, respectively. These modes all fall above the confidence interval and therefore are significant. This finding indicates that modes 2, 3 and 4 are real signals, different from random red noise. They make significant contributions to the observed geopotential height.

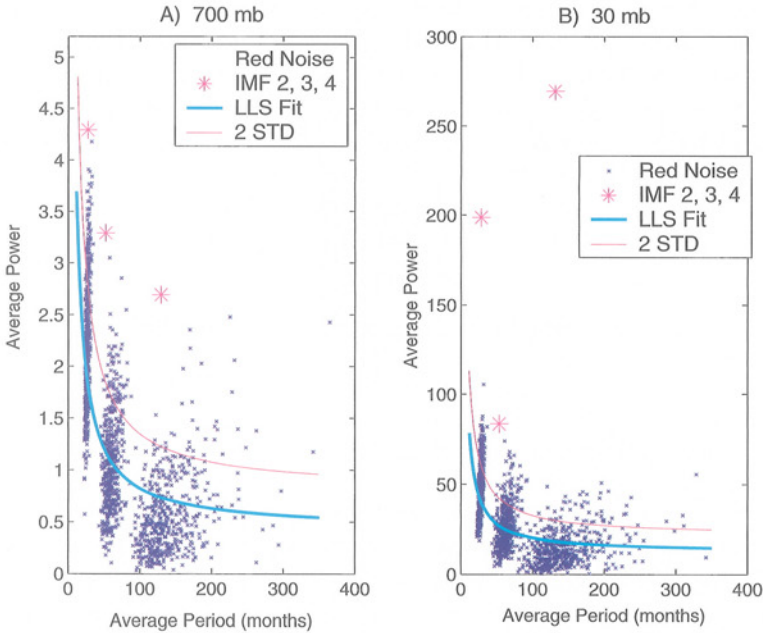


Figure 7.2: Monte-Carlo t-tests showing the significance of EMD modes. (a) 700 hPa climatolgy is added to 500 autocorrelated time series to generate a Monte-Carlo test. The red noise is calibrated by using the difference between the first mode and the climatology (Coughlin and Tung 2004a), and the autocorrelation of the noise is the same as the autocorrelation of the 700 hPa geopotential height anomalies, 0.54. These time series are decomposed by using the EMD method, and the average power in modes 2, 3 and 4 of each of the decompositions is plotted in this figure. The solid blue line represents the linear least squares fit of these points, and the red line is two standard deviations from the best-fit line. The average power of IMFs 2, 3 and 4 of the 700 hPa geopotential heights is plotted as stars. (b) Same as (a) except for the 30 hPa decomposition. Note that the 11-yr mode (IMF 4) is clearly above all random noise. Figure 7.2 was taken from Coughlin, K. T., and K. K. Tung, 2004: 11-year solar cycle in the stratosphere extracted by the empirical mode decomposition method. *Adv. Space Res.*, **34**, 323–329 with permission.

Once the significance of the mode is established, its physical relevance can be determined. Here, we use a student t-test (Hogg and Tanis 1997),

$$t = \frac{r\sqrt{N-2}}{\sqrt{1-r^2}} \quad (7.9)$$

to calculate the significance of correlations between the modes and physically relevant indices. The student t value is t , r is the correlation and $\nu = N - 2$ is the degree of freedom. Special care must be taken in estimating the degrees of freedom. Because the modes are non-stationary, typical techniques may not be applicable for finding the degree of freedom. Here, we use the following argument: In the EMD method, each IMF is successively subtracted from the original time series, leaving behind only variations with local timescales longer than those in the subtracted modes. We assume, then, that the data points in the residual time series contain

timescales equivalent to or greater than the periods of the last subtracted mode. For example, in the decomposition of the 30-hPa geopotential height, the third IMF has an average period of 4.4 yr. This finding implies that the fourth IMF is composed of data which are dependent on timescales of about 4.4 yr. Conservatively, then, we estimate that the fourth IMF has independent time intervals of 5 yr. By using this estimate, nine independent measurements of the time series can be made for the 4th IMF at 30-hPa, and, therefore, $\nu = 7$ degrees of freedom for the correlation calculation. For this example, correlations with the solar flux are calculated by comparing the data every 60 months (see Fig. 7.3). These correlations average to 0.70. For comparison, the correlation coefficient, calculated by using every month in the unsmoothed sunspot numbers, is 0.72. For this mode, the correlation is very robust. If the student t-test is used, the 0.70 correlation is statistically different from the null hypothesis of a zero correlation. Although this correlation is significant at a higher level, all of our significance testing is done at a 95% confidence level.

This statistical relationships can also be verified by using a regression with autoregressive (AR) errors. For the above example, we assume that the IMF contains the solar cycle plus an autoregressive error,

$$\text{IMF4}(t) = b[\text{SI}(t) - \mu] + e(t). \quad (7.10)$$

Here, SI is a solar cycle index defined to be the sunspot number divided by 1000. The parameters, b and μ and their variances can be found by fitting the error $e(t)$ to an $\text{AR}(p)$ process for some order p . More information about this type of method can be found in Newton (1988). For this mode, the parameter values do not change significantly for different orders; however, we find that the best fit for the errors is an autoregressive process of order 5. This order gives the parameter values of $\mu = 0.082 \pm 0.013$ and $b = 42 \pm 7$ as the best fit for this model. Since $b = 42$ is about 6 times its standard error, we can effectively rule out the hypothesis $b = 0$. This conclusion implies that the solar cycle is directly related to the fourth IMF. The regression is highly significant, and the sunspot cycle statistically explains the majority of the fourth mode. A similar type of analysis is performed for the other modes.

7.5. Results and physical interpretations

Figure 7.1 shows the complete decomposition of the 30-hPa and 700-hPa geopotential height spatially averaged over all longitudes and latitudes from 20°N to 90°N. Although the EMD modes are empirically determined, they remain locally orthogonal to one another. The time series is separated into five modes and a trend. The first IMF contains the annual cycle. The second IMF has an average period of 28 months and is anti-correlated with the equatorial QBO. The third ENSO-like mode has an average period of four years. The fourth mode, with an average period of 11 yr, is highly correlated with the solar cycle, and the trend indicates cooling in the stratosphere over time. These trends are consistent with theories of stratospheric

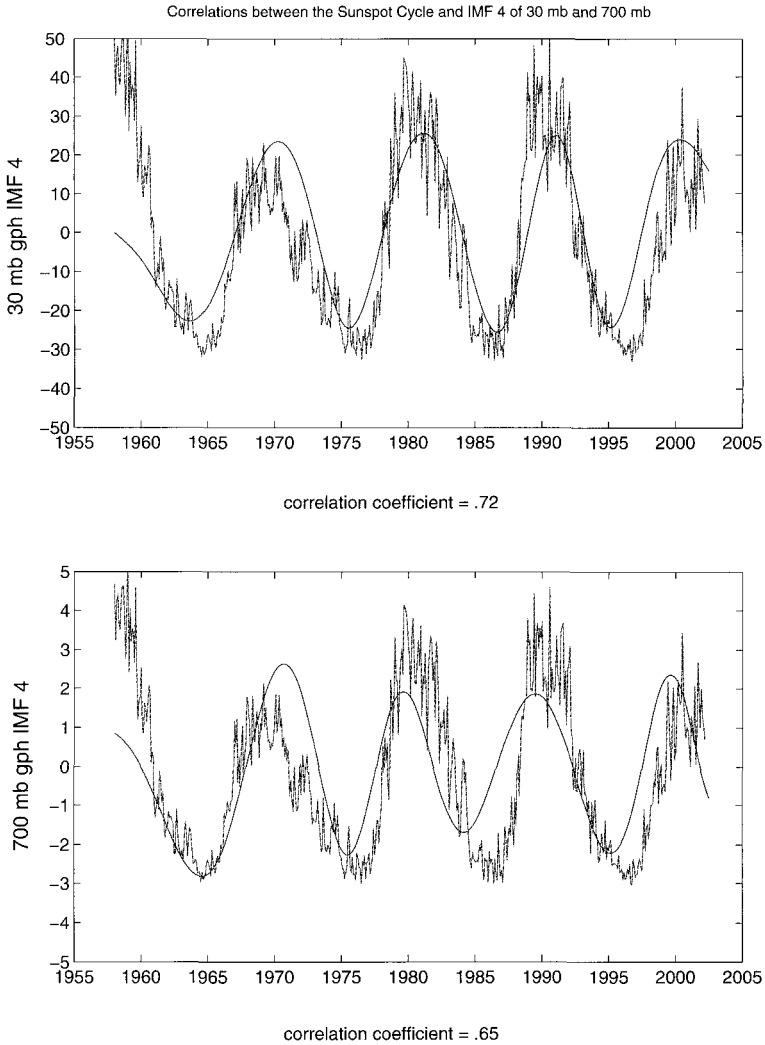


Figure 7.3: Significant correlation is 0.70 for 30 mb and 0.58 for 700 mb. Significance assumes that the mode has only 7 degrees of freedom. Figure 7.3 was taken from Coughlin, K. T., and K. K. Tung, 2004: 11-year solar cycle in the stratosphere extracted by the empirical mode decomposition method. *Adv. Space Res.*, **34**, 323–329 with permission.

cooling due to increases in greenhouse gases. Amazingly, similar decompositions are found at almost all heights and latitudes.

7.5.1. Annual cycle

Although most analysis of atmospheric data begins by subtracting a climatological mean from the time series, the winter-to-summer differences are retained in this analysis. As a result, the very first mode is always a large annual cycle. Because

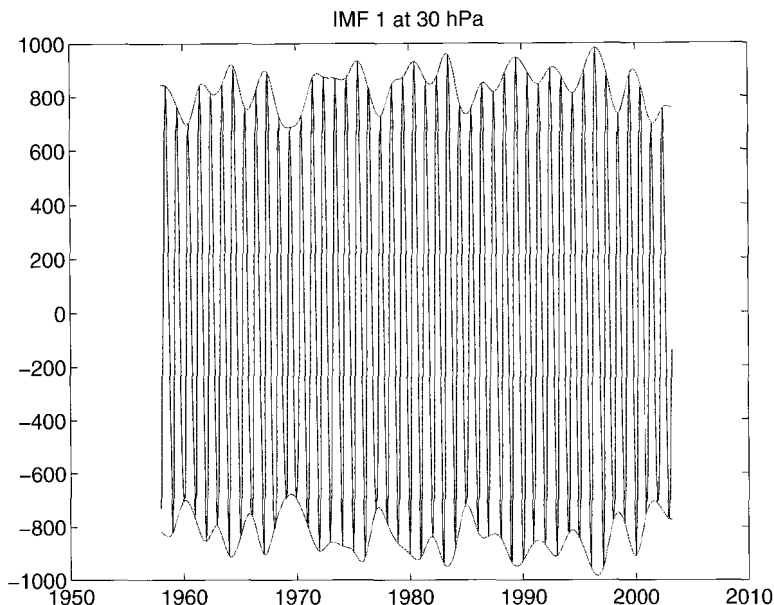


Figure 7.4: Amplitude modulations of the first mode. At 30 hPa the first IMF of the total geopotential height at the pole, from 65°N to 90°N.

the EMD method is non-stationary and nonlinear, we can look at the seasonal variations. Figure 7.4 shows that the annual cycle is not strictly regular in frequency or amplitude.

7.5.2. Quasi-Biennial Oscillation (QBO)

The second mode has an average period of 28 months and, in the extratropics, is anticorrelated with the equatorial QBO. Its see-saw pattern of geopotential height (see Holton and Tan 1980) with a node at 50°N is apparent in Fig. 7.5. The extratropical manifestation of the QBO in the stratosphere is relatively well understood: During winter, the polar geopotential height is anticorrelated with the equatorial winds due to the Holton-Tan mechanism (Holton and Tan 1980,1982; Tung and Yang 1994) and to the asymmetrical QBO direct circulation in the lower stratosphere (Jones et al. 1998; Kinnersley 1998; Kinnersley and Tung 1999). The tropospheric mechanism is not yet understood but has been observed in previous work (Coughlin and Tung 2001; Thompson et al. 2002). Here, the correlations in the troposphere are small, probably due to the short data record and the possible phase shifts associated with the influence of the equatorial QBO at various levels besides 30 hPa.

7.5.3. ENSO-like mode

The third ENSO-like mode has an interesting latitudinal and height structure. It is positively correlated with the Multivariate ENSO index in the tropical troposphere

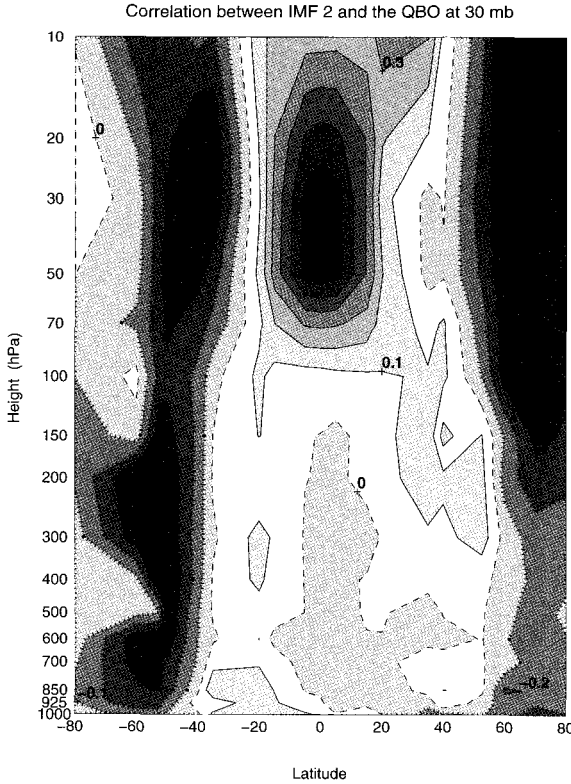


Figure 7.5: A correlation map of the second mode and the equatorial QBO. A map of correlation coefficients between the second IMF at each height latitudinal strips of 20° and the QBO Index. The coefficients are plotted at the height and mean latitude of each decomposition. The horizontal axis ranges from 40°S to 80°N .

and anticorrelated in the extratropical troposphere, between 40°N and 60°N . The signal also seems to have influence higher up into the atmosphere, both in the tropical and extratropical regions, but the correlations there are not statistically significant because a zonal average is taken here, which cancels out most of the positive and negative signals in the Pacific basin. Wu and Huang (2004) have also used EMD to analyze an ENSO signal. In general, the influence of this signal deserves further analysis.

7.5.4. Solar cycle signal in the stratosphere

The fourth IMF has the same frequency as that of the 11-yr solar cycle and also contains amplitudes comparable to those previous estimates of geopotential height solar cycle variations. More in-depth discussion of this mode can be found in Coughlin and Tung (2004a,b). In our analysis, the peak-to-peak amplitude variation of the solar cycle signal is about 50 m for the geopotential height averaged over the Northern Hemisphere at 30 hPa. In Labitzke's (2001) paper, a 3-yr running mean

of geopotential height at 30 hPa and at a selected location, 3°N/150°W, from 1958 to 1997 has peak-to-peak amplitude variations ranging from 40 to 90 meters.

Although many reports have been made of the 11-yr solar cycle in atmospheric data, a considerable debate is taking place about the spatial and temporal extent to which the atmosphere is influenced by the 11-yr variations in the solar irradiance and about the validity of the statistical significance of these claims. A major problem is the shortness of the data record, which prevents a straightforward extraction of an 11-yr signal in the energy spectrum of dynamical variables.

A small amplitude solar cycle signal has, nevertheless, been found in the quiescent regions of the dataset by previous authors. In the extratropical middle atmosphere, this signal has been found during summers (Labitzke 1987; Labitzke and van Loon 1988, 1989; Kodera 1991; Dunkerton and Baldwin 1992; van Loon and Labitzke 1994) — away from the time periods of most variability — over the mid-latitude Pacific (Gray and Ruth 1993; Haigh 2002; Labitzke 2001; Labitzke and van Loon 1992, 1994, 1999) — away from the spatial areas of the most variability — and during the westerly phases of the QBO (Labitzke 1987; Labitzke and van Loon 1988, 1994; Gary and Ruth 1993, Ruzmaikin and Feynman 2002) — away from the periods of the most dynamical disturbance.

During these quiescent periods of time and in quiescent regions of space, the stratosphere is observed to be positively correlated with the solar cycle. What we find (see Coughlin and Tung 2004a,b) is a solar cycle signal in a more general and global sense, without resorting to any specific grouping of the data, either by season, area or the phase of the QBO. This consideration is important in the test for the statistical significance of the signal, as the stratospheric record is short with less than five cycles of the solar signal. The spatial structure of the fourth mode is shown in Fig. 7.6. From these correlations, we see that a component of the climate is always in sync with the solar cycle. In the region between 50°S and 50°N, the coherence between the atmospheric signal and the solar flux is robust. These solar signals are constant in amplitude and have very little latitudinal or vertical variation. At the poles, the signal is less robust, perhaps because of poor data quality at the poles, or because of a real difference in this region. We reserve that analysis for future investigation.

The correlation map in Fig. 7.6 shows statistically how closely these signals are related to the solar flux. The solar flux is positively correlated with the fourth mode almost everywhere in our domain (see Fig. 7.6). In contrast to mode 2 (Fig. 7.5) and mode 3, which have interesting spatial structures, mode 4 is comparatively uniform. The only minor exception is in the south polar region, and the correlations there are not statistically significant.

7.5.5. *Fifth mode*

The fifth IMF contains only one or two oscillations, and little is known about it. Some researchers have speculated that it may be related to a double solar period

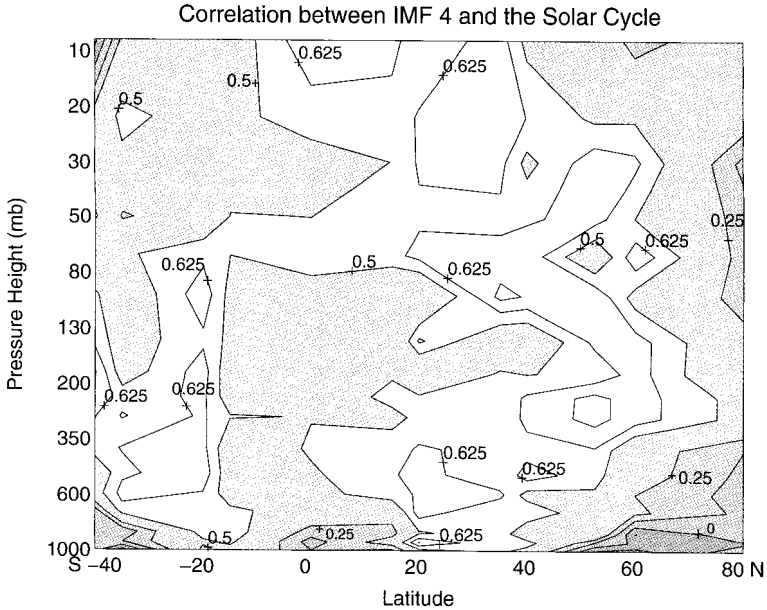


Figure 7.6: A correlation map of the fourth mode and the solar flux. A map of correlation coefficients between the fourth mode of each latitudinal strip and the solar flux. The coefficients are plotted at the pressure altitude and mean latitude of each decomposition. The horizontal axis ranges from 40°S to 80°N. Figure 7.6 was taken from Coughlin, K. T., and K. K. Tung, 2004: 11-year solar cycle in the stratosphere extracted by the empirical mode decomposition method. *Adv. Space Res.*, **34**, 323–329 with permission.

or to the Pacific Decadal Oscillation (PDO), but correlations show that it probably is not. Moreover, although it is correlated with the double solar cycle, it is not statistically significant because we only have two such periods. Another theory is that this mode may actually be physically associated with the trend. In that case, it might represent further nonlinearities in the anthropogenic influences on the atmosphere. For now, however, we reserve further comment until these possibilities can be distinguished from one another.

7.5.6. Trends

The trends, as seen in Fig. 7.1, are very robust in that the stratosphere exhibits cooling, and the troposphere has experienced warming over the last few decades. This finding is consistent with the anticipated effect of recent increases in greenhouse gases.

7.6. Conclusions

Through the EMD representation, we are able to see the natural variations in the atmosphere. This method is both compact and complete. We are able to completely

describe the changes in the lower atmosphere with only 5 modes and a trend. Each of these modes is empirically determined and not artificially constrained to have fixed amplitudes or frequencies. Furthermore, the statistically significant modes can be identified with known physical phenomena. Here, this ability allows us to gain a straightforward view of our climate, its components and the temporal/spatial distribution of these physical phenomena. The signals occur almost everywhere in the lower atmosphere (Figs. 7.5 and 7.6). We find that the significant inter-annual atmospheric modes include the QBO mode, the ENSO-like mode, the solar cycle, and climate trends that are consistent with the increases in greenhouse gases.

Acknowledgments

We thank Dr. Zhaohua Wu for first introducing us to the EMD method, and we thank Dr. Dean Duffy for his meticulous editing and typesetting. This research was supported by the National Science Foundation, Climate Dynamics Program, under grant ATM-0332364.

References

- Coughlin, K. T., and K. K. Tung, 2001: QBO signal found at the extratropical surface through northern annular modes. *Geophys. Res. Lett.*, **28**, 4563–4566.
- Coughlin, K. T., and K. K. Tung, 2004a: 11-year solar cycle in the stratosphere extracted by the empirical mode decomposition method. *Adv. Space Res.*, **34**, 323–329.
- Coughlin, K., and K. K. Tung, 2004b: Eleven-year solar cycle signal throughout the lower atmosphere. *J. Geophys. Res.*, **109**, D21105, doi:10.1029/2004JD004873.
- Dunkerton, T. J., and M. P. Baldwin, 1992: Modes of interannual variability in the stratosphere. *Geophys. Res. Lett.*, **19**, 49–52.
- Flandrin, P., G. Rilling, and P. Gonçalvès, 2004: Empirical mode decomposition as a filter bank. *IEEE Signal Process. Lett.*, **11**, 112–114.
- Gray, L. J., and S. Ruth, 1993: The modeled latitudinal distribution of the ozone quasi-biennial oscillation using observed equatorial winds. *J. Atmos. Sci.*, **50**, 1033–1046.
- Haigh, J. D., 2002: The effects of solar variability on the Earth's climate. *Philos. Trans. R. Soc. London, Ser. A*, **361**, 95–111.
- Hogg, R. V., and E. A. Tanis, 1997: *Probability and Statistical Inference*. Prentice Hall, 722 pp.
- Holton, J. R., and H. C. Tan, 1980: The influence of the equatorial quasi-biennial oscillation on the global circulation at 50 mb. *J. Atmos. Sci.*, **37**, 2200–2208.
- Holton, J. R., and H. C. Tan, 1982: The quasi-biennial oscillation in the Northern Hemisphere lower stratosphere. *J. Meteor. Soc. Japan*, **60**, 140–148.
- Huang, N. E., Z. Shen, S. R. Long, M. C. Wu, H. H. Shih, Q. Zheng, N.-C. Yen, C. C. Tung, and H. H. Liu, 1998: The empirical mode decomposition and the

- Hilbert spectrum for nonlinear and non-steady time series analysis. *Proc. R. Soc. London, Ser. A*, **454**, 903–995.
- Huang, N. E., Z. Shen, and S. R. Long, 1999: A new view of water waves – The Hilbert spectrum. *Ann. Rev. Fluid Mech.*, **31**, 417–457.
- Jones, D. B. A., H. R. Schneider, and M. B. McElroy, 1998: Effects of the quasi-biennial oscillation on the zonally averaged transport of tracers. *J. Geophys. Res.*, **103**, 11235–11249.
- Kalnay, E., and Coauthors, 1996: The NCEP/NCAR 40-year reanalysis project. *Bull. Amer. Meteor. Soc.*, **77**, 437–471.
- Kinnersley, J. S., and K. K. Tung, 1999: Mechanisms for the extratropical QBO in circulation and ozone. *J. Atmos. Sci.*, **56**, 1942–1962.
- Kodera, K., 1991: The solar and equatorial QBO influences on the stratospheric circulation during the early Northern Hemisphere winter. *Geophys. Res. Lett.*, **18**, 1023–1026.
- Labitzke, K., 1987: Sunspots, the QBO, and the stratospheric temperature in the north polar region. *Geophys. Res. Lett.*, **14**, 535–537.
- Labitzke, K., and H. van Loon, 1988: Associations between the 11-year solar cycle, the QBO and the atmosphere: I. The troposphere and stratosphere in the Northern Hemisphere winter. *J. Atmos. Terr. Phys.*, **50**, 197–206.
- Labitzke, K., and H. van Loon, 1989: The 11-year solar cycle in the stratosphere in the northern summer. *Ann. Geophys.*, **7**, 595–597.
- Labitzke, K., and H. van Loon, 1992: On the association between the QBO and the extratropical stratosphere. *J. Atmos. Terr. Phys.*, **54**, 1453–1463.
- Labitzke, K., and H. van Loon, 1994: Trends of temperature and geopotential height between 100 and 10 hPa on the Northern Hemisphere. *J. Meteor. Soc. Japan*, **72**, 643–652.
- Labitzke, K., and H. van Loon, 1999: *The Stratosphere: Phenomena, History, and Relevance*. Springer, 179 pp.
- Labitzke, K., 2001: The global signal of the 11-year sunspot cycle in the stratosphere: Differences between solar maxima and minima. *Meteor. Z.*, **10**, 83–90.
- Mak, M., 1995: Orthogonal wavelet analysis: Interannual variability in the sea surface temperature. *Bull. Amer. Meteor. Soc.*, **76**, 2179–2186.
- Newton, H. J., 1988: *TIMESLAB: A Time Series Analysis Laboratory*. Wadsworth and Brooks/Cole Publishing Co., 625 pp.
- Oh, H.-S., C. M. Ammann, Ph. Naveau, D. Nychka, and B. L. Otto-Bliesner, 2003: Multi-resolution time series analysis applied to solar irradiance and climate reconstructions. *J. Atmos. Solar-Terr. Phys.* **65**, 191–201.
- Naujokat, B., 1986: An update of the observed quasi-biennial oscillation of the stratospheric winds over the tropics. *J. Atmos. Sci.*, **43**, 1873–1877.
- Ruzmaikin, A., and J. Feynman, 2002: Solar influence on a major mode of atmospheric variability. *J. Geophys. Res. - Atmos.*, **107**, Art. No. 4209.
- Sonechkin, D. M., and N. M. Datsenko, 2000: Wavelet analysis of nonstationary

- and chaotic time series with an application to the climate change problem. *Pure Appl. Geophys.*, **157**, 653–677.
- Thompson, D. W. J., M. P. Baldwin, and J. M. Wallace, 2002: Stratospheric connection to Northern Hemisphere wintertime weather: Implications for prediction. *J. Climate*, **15**, 1421–1428.
- Tung, K. K., and H. Yang, 1994: Global QBO in circulation and ozone. Part I: Reexamination of observational evidence. *J. Atmos. Sci.*, **51**, 2699–2707.
- Van Loon, H., and K. Labitzke, 1994: The 10-12-year atmospheric oscillation. *Meteor. Z.*, **3**, 259–266.
- Wolter, K., 1987: The Southern Oscillation in surface circulation and climate over the Atlantic, Eastern Pacific, and Indian Oceans, as captured by cluster analysis. *J. Climate Appl. Meteor.*, **26**, 540–558.
- Wolter, K., and M. S. Timlin, 1993: Monitoring ENSO in COADS with a seasonally adjusted principal component index. *Proc. 17th Climate Diag. Workshop*, Norman, OK, pp. 52–57.
- Wolter, K., and M. S. Timlin, 1998: Measuring the strength of ENSO event: How does 1997/98 rank? *Weather*, **53**, 315–324.
- Wu, Z., and N. E. Huang, 2004: A study of the characteristics of white noise using the empirical mode decomposition method. *Proc. R. Soc. London, Ser. A*, **460**, 1597–1611.
- Zhu, X., Z. Shen, S. D. Eckermann, M. Bittner, I. Hirota, and J.-H. Yee, 1997: Gravity wave characteristics in the middle atmosphere derived from the empirical mode decomposition method. *J. Geophys. Res.*, **102**, 16545–16561.

Katie Coughlin

University of Washington, Department of Applied Mathematics, Box 352420, Seattle, WA 98195, USA

katie@amath.washington.edu

Ka Kit Tung

University of Washington, Department of Applied Mathematics, Box 352420, Seattle, WA 98195, USA

tung@amath.washington.edu